Intrusion of lamprophyre dyke and related deformation effects in the host rock salt: a case study from the Loulé diapir, Portugal

M. Machek[a], Z. Roxerová[a], P. Závada[a], P.F. Silva[b], B. Henry[c], P. Dědeček[a], E. Petrovský[a], F.O. Marques[d]

[a] *Institute of Geophysics AS CR, v.v.i, Boční II/1401, 14131, Prague 4, Czech Republic, mates@ig.cas.cz*
[b] *ISEL and IDL (Univ. Lisbon), Lisbon, Portugal*
[c] *Paléomagnétisme, Institut de Physique du Globe de Paris, Sorbonne Paris Cité, Université Paris Diderot, UMR 7154 CNRS, Saint- Maur cedex, France*
[d] *Universidade de Lisboa, Lisboa, Portugal*

Article in press, Tectonophysics (2014)

A rock salt – lamprophyre dyke contact zone (sub-vertical, NE-SW strike) was investigated for its petrographic, mechanic and physical properties by means of anisotropy of magnetic susceptibility (AMS) and rock magnetic properties, coupled with quantitative microstructural analysis and thermal mathematical modelling. The quantitative microstructural analysis of halite texture and solid inclusions revealed good spatial correlation with AMS and halite fabrics. The fabrics of both lamprophyre and rock salt record the magmatic intrusion, "plastic" flow and regional deformation (characterized by a NW-SE trending steep foliation). AMS and microstructural analysis revealed two deformation fabrics in the rock salt: (1) the deformation fabrics in rock salt on the NW side of the dyke are associated with high temperature and high fluid activity attributed to the dyke emplacement; (2) On the opposite side of the dyke, the emplacement-related fabric is reworked by localized tectonic deformation. The paleomagnetic results suggest significant rotation of the whole dyke, probably during the diapir ascent and/or the regional Tertiary to Quaternary deformation.

1 Introduction

The relationship between a dyke and its host rock in the upper crust is formally described as the propagation of a fluid-filled fracture in a linear elastic medium (Rubin, 1993; 1995), while inelastic deformation in the host rock, resulting in a variety of brittle deformation features, characterizes the shallow crustal levels (Baer, 1991; Correa-Gomes et al., 2001; Pollard, 1987; Rubin, 1993; Weinberger and Bear, 1995). However, in some mechanically weak rock types, especially in rock salt, the upward curvature of rock salt layers adjacent to the dyke indicates a viscous drag accommodated by recrystallization in ductile creep regimes (Knipping,1989). The magma flowing through the dyke conduit modifies the conditions in the narrow zone of the host rock in terms of stress field, fluid activity and temperature, which can cause deformation and melting of the host rock (Knipping, 1989). This type of contact zone can contribute to the understanding of the magma ascent in deeper crustal levels, and also to the description of deformation mechanisms of the rock salt at high temperature. The mechanisms of such ductile deformation in the vicinity of a dyke have not yet been studied in detail.

The deformational behaviour of rock salt depends on temperature, confining pressure, grain size and solid solution impurities and is strongly stimulated by the presence of fluid at the grain boundaries (e.g. Marques et al., 2013; Pennock et al., 2006a,b, 2005; Schléder and Urai 2007; Schléder et al., 2007; Ter Heege et al., 2005a,b; Trimby et al., 2000; Urai et al., 2008; Urai et al. 1987; Wenk et al., 2009). The quantitative characterization of the fabrics is a necessary prerequisite for identifying the combined influence of the above stated physical conditions, and correct extrapolation of the deformation mechanisms from the conditions of experimental deformation (e.g. Desbois et al., 2010; Passchier and Trouw, 2005; Urai et al., 2008;). The lack of visible strain markers in rocks is nowadays often compensated by the determination of their low-field anisotropy of magnetic susceptibility (AMS; for review see Borradaile and Henry, 1997; Borradaile and Jackson, 2010; Hrouda, 1982; Tarling and Hrouda, 1993). AMS has a great potential to reveal the internal fabric in rock salt, despite the very weak magnetic susceptibility. There are very few studies on the magnetic fabric of rock salt (e.g. Hrouda et al., 2001, 2004), therefore this is a unique opportunity.

The present paper reports on a detailed study of the interaction between the intrusion of a dyke in salt rock and the structural evolution in the Loulé Salt Mine in Southern Portugal. We used a combination of magnetic studies (comprising AMS, rock magnetism and paleomagnetism) with the quantification of rock microstructure (from the lattice and shape preferred orientation). The aim of this work is to pinpoint and characterize the internal fabrics promoted in the host rock salt by dyke intrusion and subsequent deformation processes.

An AMS study was first performed, as it is a fast and effective method to determine orientation and strength of rock fabric. The tectonic evolution of the salt/dyke system after the dyke intrusion was also characterized by means of paleomagnetism. The quantified rock salt microstructure has been compared with the AMS data. A detailed microstructural description together with the CPO provided information about conditions and processes that led to salt fabric formation. Finally to confirm or disprove the deduced deformation mechanisms and conditions, mathematical modeling of the temperature field inside and outside the dyke after its intrusion was carried out.

2 Geological setting

The Loulé salt diapir in the Mesozoic-Cenozoic Algarve basin (Fig. 1a) was chosen as case study to show the relationship between mafic dyke emplacement and host rock salt deformation. This basin, consisting of two superimposed Mesozoic and Cenozoic sedimentary sequences (Terrinha, 1998), is the outermost geological province of southern Portugal. It is mainly filled by marine limestones, marls and sandstones accumulated during the Late Triassic to Quaternary. In addition, it comprises Hettangian evaporites interbedded with siliceous sediments of a volcano sedimentary complex. The basin developed as a result of extensional tectonics associated with the break up of Pangaea

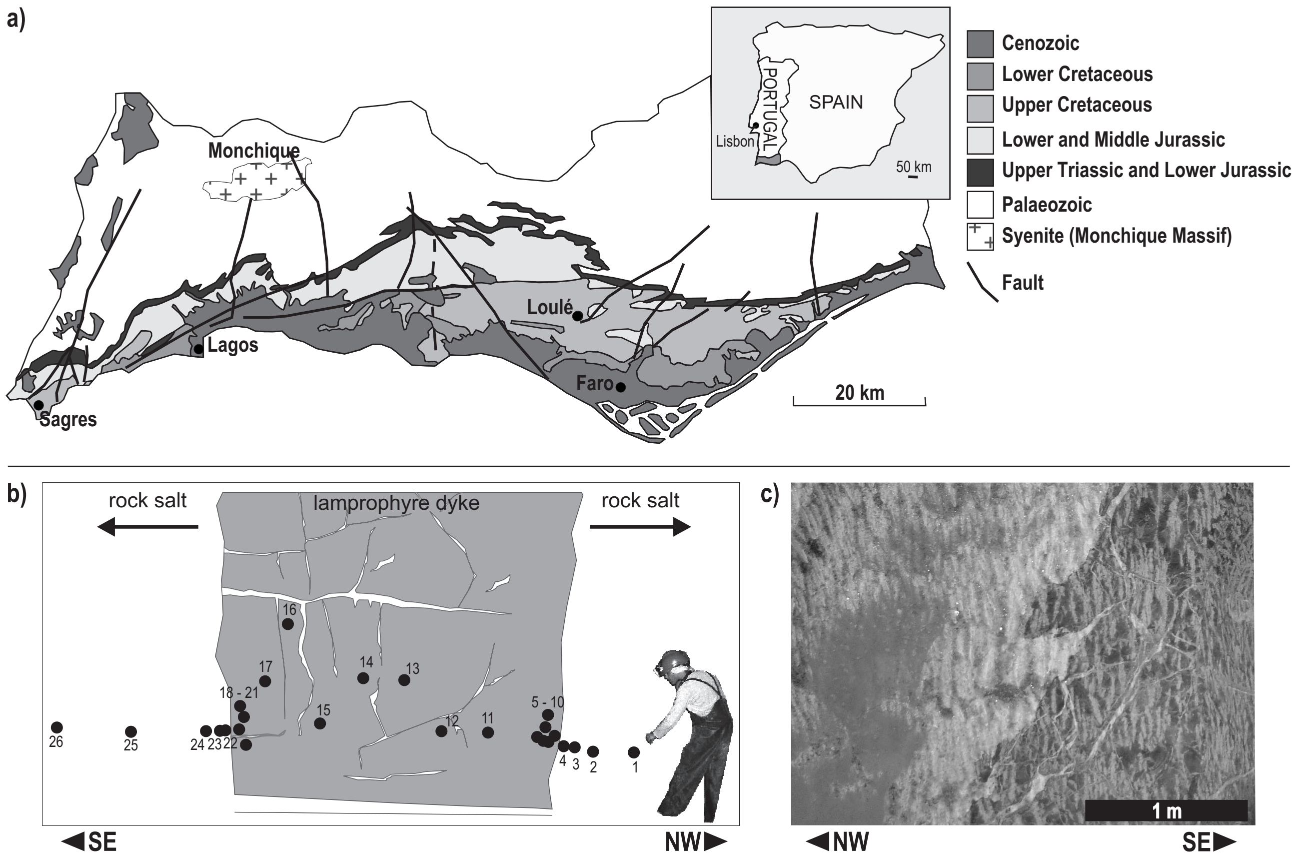

Figure 1 *Geology of the studied area. a) Simplified geological map showing the location and regional geology of the Algarve basin after Borges et al. (2012). b) Position of profile within the dyke and salt-rock system and the numbers and position of individual samples. c) Detailed photographs of the contact between the rock salt and the lamprophyre dyke.*

and development of the westernmost Neo Tethys from Early Triassic to Late Cretaceous times (Terrinha, 1998). The first stage of deformation during the Middle Jurassic (the Dogger) resembles the extension of crustal tectonic blocks, promoting a downward movement of salt along an inclined surface, forming recumbent folds with horizontal thrust sub-vergence (Terrinha et al., 1994). Later, during the Campanian (Miranda et al., 2009), the evaporites were intruded by lamprophyre dykes that belong to a small group of alkaline intrusive rocks, geochemically similar to that of the nearby Monchique complex (Martins, 1991). For the dykes, the crystallization age is 72 Ma based on K Ar biotite dating (Miranda et al., 2009). According to Terrinha (1990) and Terrinha et al. (1994), the diapiric ascent of the salt body possibly dates from the Upper Cretaceous to Early Tertiary. Finally, the Loulé diapir records Tertiary to Quaternary deformation related to a N S shortening associated with an E W regional extension, resulting in a penetrative fabric in the salt rocks.

The studied lamprophyre dyke is 3 m thick, and has an orientation 330º/80º (dip direction/dip). At both dyke margins, the texture is aphanitic with devitrified volcanic glass and abundant euhedral as well as skeletal xenocrysts of olivine and olivine xenoliths, with serpentinized olivine xenocrysts at the SE margin. The dyke centre shows subophitic texture of plagioclase laths, needle crystals of amphibole and large anhedral crystals of biotite, with high amount of volcanic glass. The olivine xenocrysts are significantly less abundant in the dyke core. Only brittle structures have been observed in the dyke itself (Fig. 1b). Fractures within the dyke are filled with halite. Within the host salt rock close to the SE dyke margin, angular fragments of lamprophyre of various sizes can be observed. In the same area, smaller dykes appear strongly dismembered within the salt.

Samples were collected in rock salt and within and around a lamprophyre dyke in the Loulé Mine. Core samples were obtained using a gasoline-powered portable drill (profiting the very efficient ventilation inside the mine) and oriented with a magnetic compass. A profile across the host rock salt and dyke was sampled in detail (Fig. 1b). The salt rock was sampled on the NW and SE sides of the dyke, between a distance of 5 to 220 cm and 10 to 75 cm of dyke margins, respectively. The dyke was also sampled along a complete cross-section. Additionally, the regional salt (hosting the dyke) was sampled in three distinct stations, each one sampled along several tens of meters and at the distance of 200 - 300 m from the studied dyke.

3 Rock magnetism

Detailed magnetic mineralogy studies were carried out, comprising thermomagnetic and classical hysteresis analyses.

3.1 Bulk Magnetic Susceptibility

The measurements of bulk magnetic susceptibility were carried out on a KLY-4S Kappabridge (Hrouda, 1994; Jelínek and Pokorný, 1997) at the Institute of Geophysics in Prague. In the rock salt away from dykes, the mean susceptibility k_m (measured on 108 specimens; between 1 to 3 drill cores per site) is very low, ranging from -13×10^{-6} SI to 69×10^{-6} SI, with median value -7×10^{-6} SI. The rock salt in the vicinity of the dyke shows km clustering around 0.3×10^{-6} SI. However, towards the SE margin, the km value increases from -9×10^{-6} SI at one meter from the dyke margin to 445×10^{-6} SI at the contact. In the dyke (42 specimens), km is high, with a median value of 52×10^{-3} SI. The mean susceptibility increases towards the centre of the dyke, from 39×10^{-3} SI to 79×10^{-3} SI.

3.2 Thermomagnetic analyses

Thermomagnetic analysis (measurement of bulk magnetic susceptibility as a function of temperature – $k_b(T)$) was carried out under non-controlled atmosphere on powdered specimens using the CS-3 Furnace and/or the CS-L Cryostat Apparatus, and the KLY-4S Kappabridge (Hrouda, 1994; Jelínek and Pokorný, 1997) at the Institute of Geophysics in Prague. $k_b(T)$ values were obtained for the rock salt, the dyke, and dyke fragments found within the salt. The thermomagnetic curves of host rock salt present in general much more "noise" (Fig.2) than those from the lamprophyre dyke. That is related to high susceptibility in dyke rocks compared to the very low signal from rock salt.

The host rock salt exhibits a slight decrease in k_b below 0 °C, and a constant trend of negative k_b above 0 °C, suggesting a diamagnetic type of k_b-T relationship characteristic for halite (Fig. 2a). Towards the NW dyke margin, the thermomagnetic curves reveal a more hyperbolic character at low temperatures (Fig. 2c), in agreement with the presence of paramagnetic sedimentary admixture.

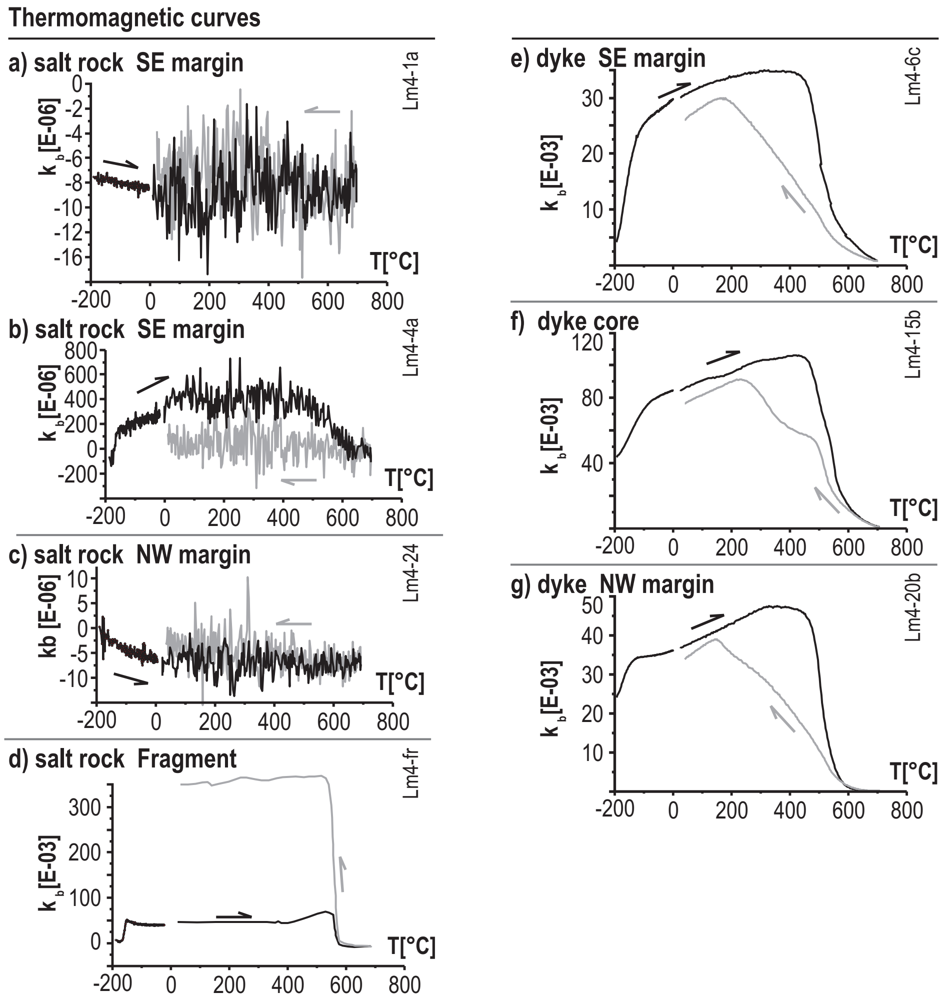

Figure 2. *Diagram of bulk magnetic susceptibility (k_b) versus temperature (T) for low and high temperatures. a) and b) thermomagnetic curves for the rock salt on SE margin; c) thermomagnetic curve of salt rock from the NW margins; d) thermomagnetic curve of the dyke fragment in the salt; e) thermomagnetic curve from SE dyke margin; f) center of the dyke; g) NW dyke margin. Heating curves are black and cooling curves are gray. The scale in diagram differs due to large magnetic susceptibility range of measured samples.*

Close to the SE margin, the Verwey transition is observed around -150 ºC (Verwey, 1939), and a sharp decay at high temperatures (~580 °C), both characteristics indicating the presence of magnetite (Fig. 2b). The rock salt thermomagnetic analysis thus reveals the combined signal of dia, para and ferrimagnetic minerals.

The lamprophyre (dyke and fragments found in the nearby rock salt) exhibits a magnetite type of thermomagnetic behaviour, i.e., sharp Verwey transition and abrupt decay around 580 ºC (Fig. 2d). Between the Verwey transition and 580 ºC, the sampled fragment mostly shows stable susceptibility values, and a cooling curve with higher values. Dyke samples from both margins and core show quite similar susceptibility evolution with temperature (Fig. 2e - g), but distinct from the isolated fragment embedded in the salt. During progressive heating, a Verwey transition is responsible for a significant increase of susceptibility values until -100 ºC. Above this temperature, the susceptibility gradually increases until 500 – 530 ºC, followed by a sharp drop with a smooth hyperbolic decay above 580 ºC. At this final drop, the sample from the core shows a stepwise decay (Fig. 2f), which is not observed for samples from the dyke margins (Fig. 2e,g). The shape of the thermomagnetic curves suggests the presence of magnetite and Ti-poor titanomagnetite in dyke samples. The irreversibility of the heating and cooling $k_b(T)$ curves above room temperature indicates some mineralogical alteration, likely contemporaneous of the final cooling stages (Ade-Hall et al, 1971; Wilson et al., 1968). The hyperbolic decrease at high temperature can be related either to the paramagnetic behaviour the dyke rock forming minerals.(e.g. biotite, amphibole and olivine), or to the presence of hematite neo-formed during experimental heating (e.g., Dunlop and Özdemir, 1997). In addition, the bulk susceptibility values are slightly lower after the heating-cooling cycle than before (Figs. 2e - g), suggesting that no new magnetite was formed during this cycle.

3.3 Hysteresis loops

In order to better specify the physical properties of the studied samples, the hysteresis and remanent parameters were also measured with a Vibrating Sample Magnetometer (Model EV9 VSM, DSM Magnetics; ADE Corporation, Lowell, MA, USA) at the Institute of Geophysics in Prague. The hysteresis loops and remanent coercive force were measured (in the range from -2000 mT to 2000 mT) on crushed samples.

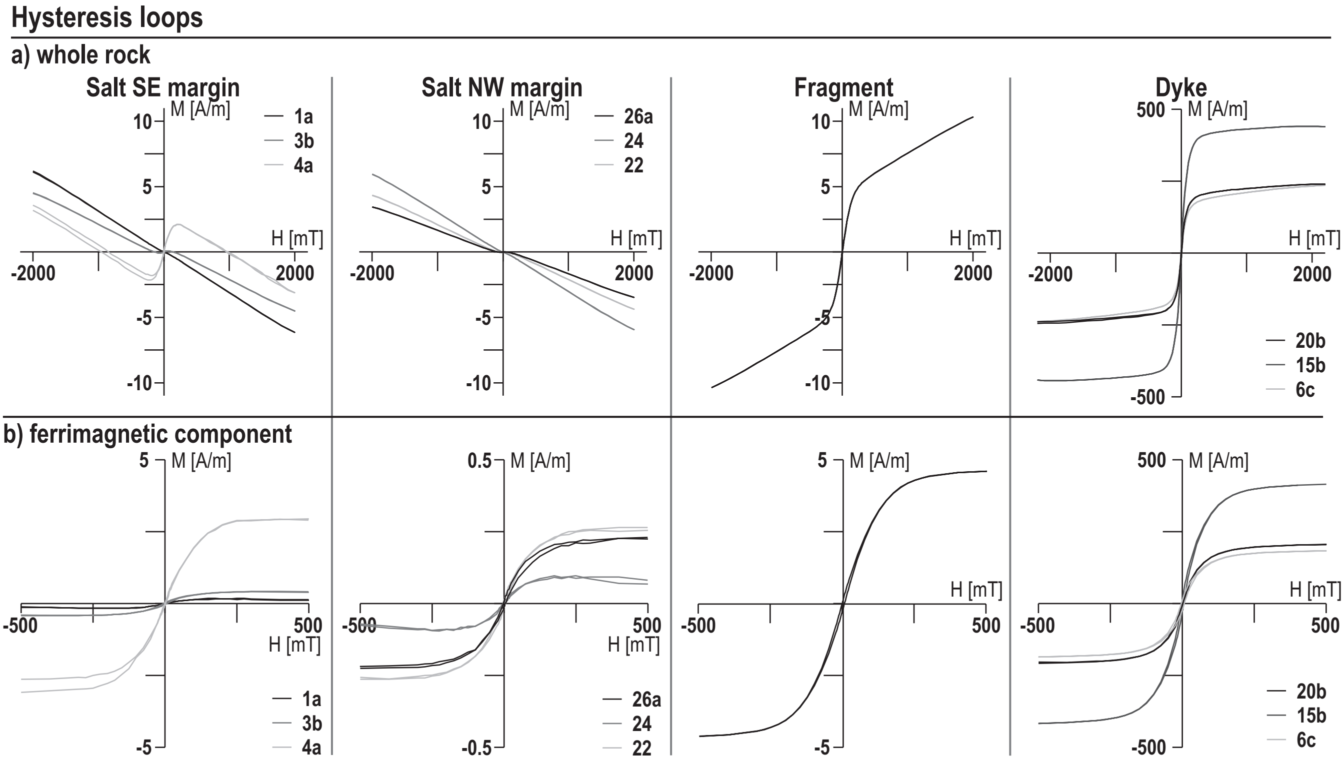

Figure 3. *Hysteresis loops. The names relating to variable colored lines refer to individual samples. M - magnetization in A/m. H - applied magnetic field intensity in mT. a) Hysteresis loops measured for the rock salt samples, dyke samples and fragment. b) The second line represents the hysteresis loops after correction for the dia/paramagnetic signal by subtracting the linear part of the hysteresis curves. The scale in diagram differs due to large magnetization values range of measured samples.*

The hysteresis curves of rock salt specimens are dominantly controlled by a linear signal with negative slope, indicating the predominance of diamagnetic minerals (Fig. 3a, sample 4a). At the SE side of the dyke, the influence of a notable ferrimagnetic component increases with proximity to the dyke wall (Fig. 3a). After correction for the dia/paramagnetic signal by subtracting the linear part of the hysteresis curves, a weak ferrimagnetic component was revealed in all the salt specimens (Fig. 3b). The hysteresis loops of the angular dyke fragment retrieved from rock salt sample 3 (50 cm away from the SE margin of the dyke) and from dyke specimens show a dominantly ferrimagnetic character (Fig. 3).

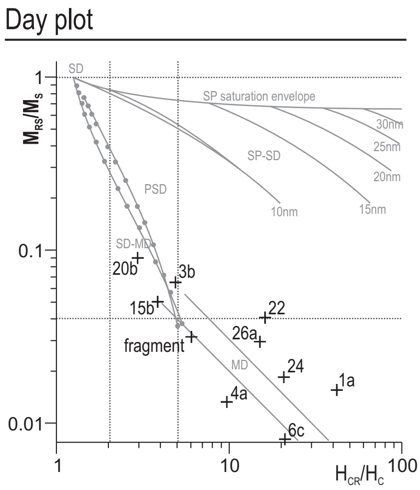

Figure 4. *Modified Day plot (Day et al., 1977; Dunlop, 2002) based on values of saturation magnetization (M_S), saturation remanence (M_{rs}), coercive force (H_C) of hysteresis loop and remanent coercive force (H_{cr}) of samples from dyke SE margin (6c), center (15b), and NW margin (20b),from salt rock from SE (1a, 3b, 4a) and NW (22, 24, 26a) sides of the dyke and from the angular rock fragment found in the salt rock.*

The shape of the hysteresis curves, corrected for the dia/paramagnetic signal by subtracting the linear part suggests the presence of a low coercivity component, like magnetite, in all salt and dyke specimens. The coercivity measured for the lamprophyre rock fragment and in two dyke specimens (6c and 15b, from dyke SE margin and core, respectively) is however slightly higher than expected for pure magnetite, likely indicating increased oxidation of titanomagnetite (Wang and Van der Voo, 2004). The ratios of saturation remanence to saturation magnetization (M_{rs}/M_s) and remanent coercive force to coercive force (H_{cr}/H_c) on a modified Day plot (Day et al., 1977; Dunlop, 2002) indicate a multi-domain (MD) character of magnetic particles prevailing in all specimens (Fig. 4), therefore an inverse fabric is not expected.

4 Anisotropy of magnetic susceptibility - AMS

The low field anisotropy of magnetic susceptibility (AMS) was measured with a MFK1-FA Kappabridge (Jelínek and Pokorný, 1997) in the field of 200 A/m and for a frequency of 976 Hz at Instituto Dom Luiz – Univiversity of Lisbon, Portugal. The data were statistically evaluated using the Anisoft 4.2. package of programs (Chadima and Jelínek, 2008; Hrouda et al., 1990; Jelínek, 1978) and are stored at PANGEA (http://doi.pangaea.de/10.1594/PANGAEA.820353?format=html). Two AMS parameters

(Jelínek, 1981) are used to characterize the magnetic fabric defined by principal magnetic susceptibilities $k_1 \geq k_2 \geq k_3$. The intensity of preferred orientation of magnetic minerals is indicated by the degree of anisotropy $P = k_1/k_3$. The shape of the magnetic fabric is defined by the parameter $T = 2\times ln(k_1/k_2)/ln(k_2/k_3)-1$, where $0 < T < 1$ and $-1 < T < 0$ correspond to oblate and prolate shapes of AMS ellipsoids, respectively (see Tarling and Hrouda, 1993). The orientation of the pole of the magnetic foliation (k_3) and lineation (k_1) are represented on lower hemisphere equal area stereograms.

The regional rock salt set comprises 108 specimens. The AMS fabric is characterized by a NW-SE magnetic foliation dipping approximately 60º towards NE, including a mean lineation that plunges 45º to E (Fig. 5). The AMS ellipsoids in regional rock salt exhibit prolate to oblate shapes with median T value close to zero. P values show a strongly increasing trend when approaching a zero susceptibility value.

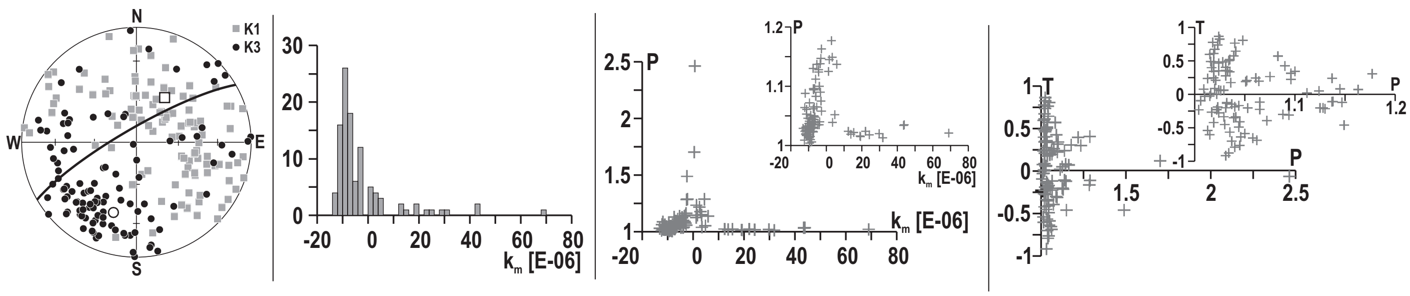

Figure 5. *AMS data of the regional rock salt collected in three distinct stations (108 specimens), at the distance of 200 – 300 m from the studied dyke. The results of AMS are presented in terms of orientation of maximum (k1, squares,) and minimum susceptibility (k3, circles) in lower hemisphere stereographic projection, km histogram, and P-km and P-T plots of all specimens. The mean orientations of k1 and k3 are represented by large open symbols. The dyke orientation (330/80) is in the stereo diagram shown as thick solid line. The small P- km and P-T plots represent a detailed inset of the data in the range of the P parameter from 1 to 1.2 to make visible the otherwise not readable data.*

4.1 AMS in the dyke

At the NW dyke margin, the AMS fabric reveals a magnetic foliation striking parallel to dyke margin (NE-SW) and steeply dipping (~80°) towards the core of the dyke (Fig. 6a). At the SE margin, the magnetic foliation is sub-parallel to the dyke wall with very steep dip towards the dyke core observed in some specimens. A prevailing sub-vertical magnetic lineation was measured at the NW margin of the dyke. At the SE margin, magnetic lineations form a girdle along the plane of magnetic foliations with maxima in the vertical direction. Towards the core of the dyke, the vertical magnetic foliation becomes sub-perpendicular to the dyke plane, and with a subhorizontal lineation. At the NW margin of the dyke, the shape of the AMS ellipsoid is characterized by high scattering of ellipsoids, from slightly oblate to prolate shapes near the contact. In contrast, the SE side shows a well clustered group of slightly oblate to neutral shapes. P is scattered around a median value $P = 1.02$ at the NW margin, without any clear pattern. The SE margin indicates a slight increase of P values towards the margin, from 1.02 to close to 1.1.

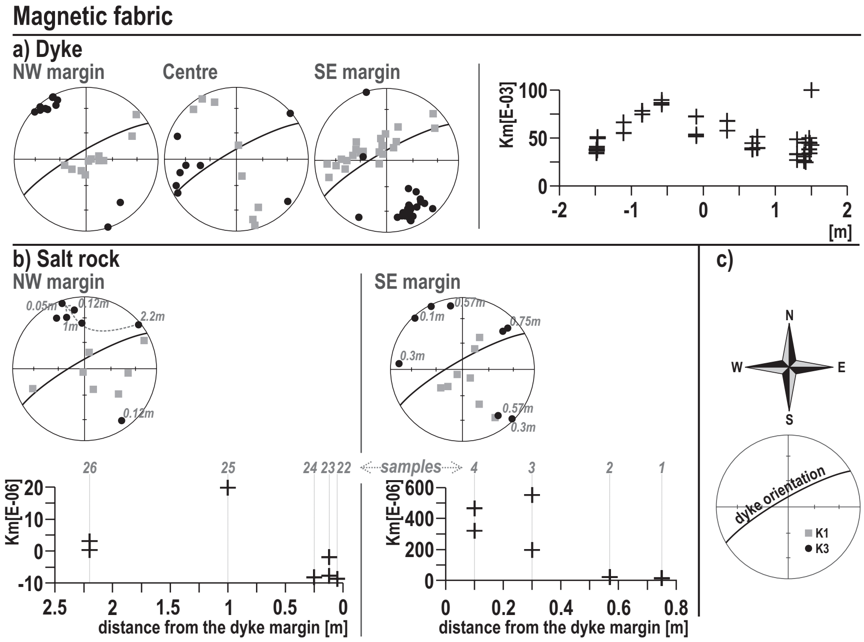

Figure 6. *Detailed AMS data. a) The orientation of the AMS results within the dyke in lower hemisphere stereographic projection showing poles to magnetic foliations (k_3, circles) and lineations (k_1, squares) and the horizontal distribution of k_m in the dyke. b) The AMS data of the salt rock sites in stereographic projection showing poles to magnetic foliations (k_3, circles) and lineations (k_1, squares) with noted distance from the dyke margins. The bottom plots show the distribution of k_m with respect to the distance from the dyke margin, labelled with sample numbers. c) Figure legend. Note different scale of k_m diagrams.*

4.2 AMS in host salt

The salt rocks hosting the dyke show an evolution of the AMS planar fabric with distance to the dyke, changing from the regional orientation to parallel with dyke, showing NE-SW subvertical magnetic foliation and subvertical lineation (Fig. 6b). However, these changes are not symmetric. Close to the NW dyke margin, the acquisition of a magnetic foliation parallel to the dyke occurs gradually, while for the SE margin it occurs more abruptly, between 0.57 and 0.75 m from the contact with the dyke. Also SE from the dyke margin, the magnetic foliation is more scattered than at the opposite side of the dyke. The highest values of P are observed for salt samples: i) carrying high k_m (around 10^{-2} SI), suggesting a compositional effect due to the presence of highly magnetic particles (Borradaile and Henry, 1997); and ii) with k_m values approaching zero, thus invalidating any attempt of quantitative interpretation (Hrouda, 2004; 1986). Regarding the shape of the ellipsoid, it varies from oblate to prolate, without clear trends along the cross sections.

5 Paleomagnetic data

In order to determine whether the dyke orientation and dyke/salt contact is tectonically disturbed, paleomagnetic experiments were conducted for both dyke and host rock salt. One-month residence time in zero-field provided the minimization of magnetic viscosity effects, after which stepwise demagnetizations were conducted by alternating field (AF) treatments, using an LDA (AGICO) demagnetizer. The remanent magnetization was measured with a JR6 (AGICO) magnetometer. Paleomagnetic directions were determined according to the Kirschvink (1980) principal components analysis. Mean site magnetization direction, its associated precision parameter (k), and radius of the angular confidence zone at 95% (α_{95}) were determined using Fisher (1953) statistics.

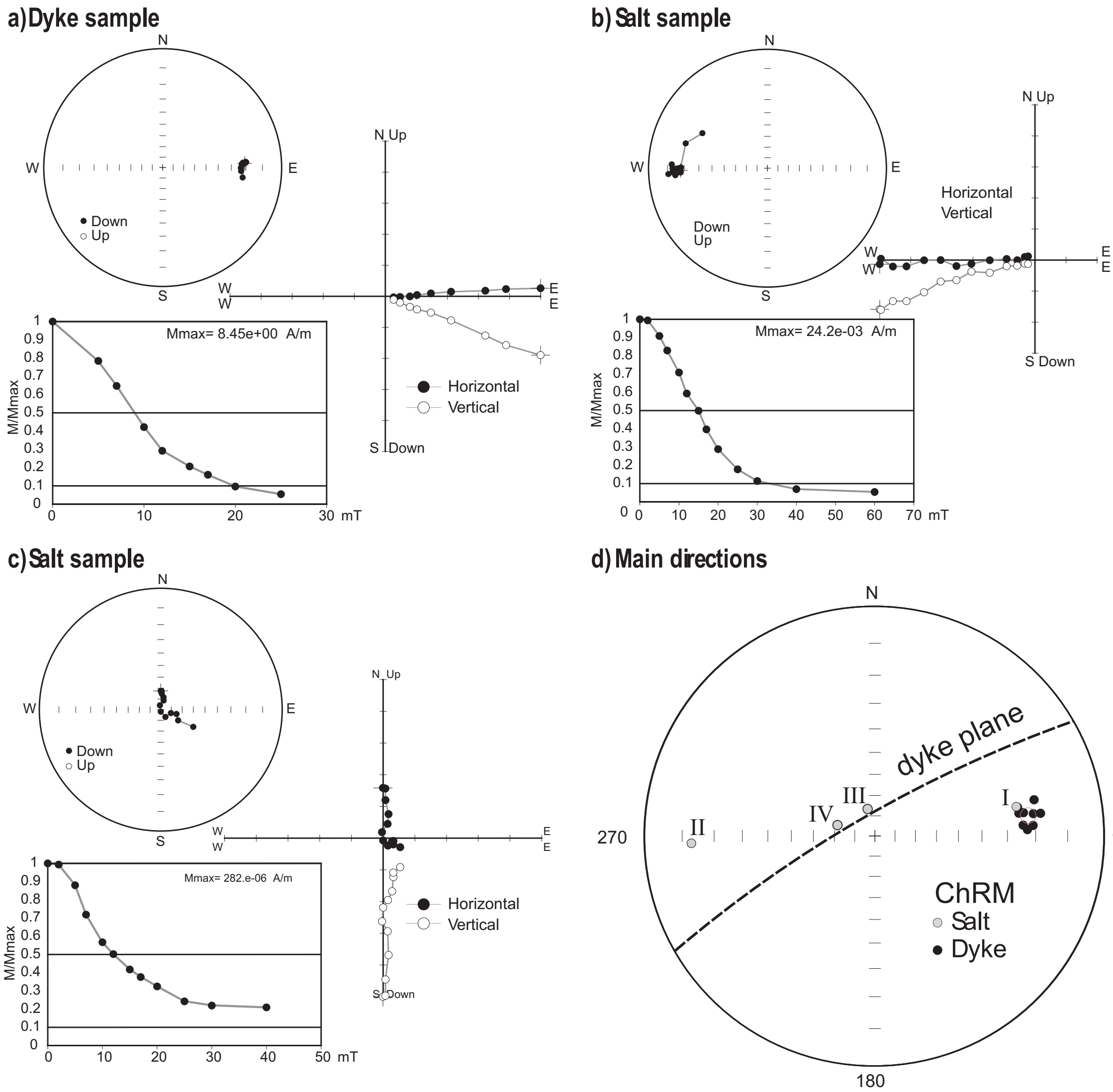

Figure 7. *Paleomagnetic data. a) Example for dyke samples; b) and c) Examples for salt rock samples; d) The main directions obtained (lower hemisphere). Salt samples position: I - sample 5 located at the SE contact; II - sample 3A located at 30 cm from the SE contact; III - sample 2B located at 57 cm from the SE contact; IV - sample 25 located at 1 m from the NW contact.*

The natural remanent magnetization (NRM) intensity of dyke samples varies between 2 and 8 A/m, while salt samples give considerable lower values, from 10^{-1} to 10^{-6} A/m. During demagnetization procedures, dyke samples show a gradual decrease in magnetization intensity, with 10% of the NRM remaining above 20 - 30 mT (Fig. 7a). This behaviour indicates the presence of a low-coercivity phase, agreeing with the rock magnetic data that indicate magnetite as the main magnetic carrier. Directional analyses mostly point out a characteristic remanent magnetization (ChRM) above 10 mT step, defining for nine samples a mean direction with *D = 81.2º, I = 22.6º, k = 321 and* α_{95}

= *2.9º* (Fig. 7d). In rock salt samples, the intensity and directions retrieved during the demagnetization procedures are much more complex. Among the seven analysed samples, only two show, during demagnetization treatment, magnetization directions converging to the axes origin of a Zijderveld diagram (ChRM), one collected at the SE contact with the dyke (D = *78.3º*, I = *25.7º*) and the other 30 cm from the same margin, giving a direction D = *267.7º*, I = *12.7º* (Fig. 7b). For these samples, less than 5% of the NRM remained between 60 and 80 mT of the applied AF. Two other samples, collected at 0.6 m and 1 m away from the dyke, yield a low coercivity secondary component (Fig. 7c). The remaining salt samples show a chaotic behaviour of the intensity of magnetization and directions. The latter much probably arises from the very low NRM values (10^{-5} to 10^{-6}) near the noise level of the magnetometer, and from acquisition of parasitic anhysteretic remanence. All the obtained paleomagnetic data can be included in an almost sub-vertical E-W plane, with pole at 175º/10º.

6 Salt microstructure

The microstructure of rock salt (Fig. 8) adjacent to the lamprophyre dyke was studied in order to directly document orientation of the rock fabric in relation to AMS, and to determine conditions and processes that led to salt fabric formation.

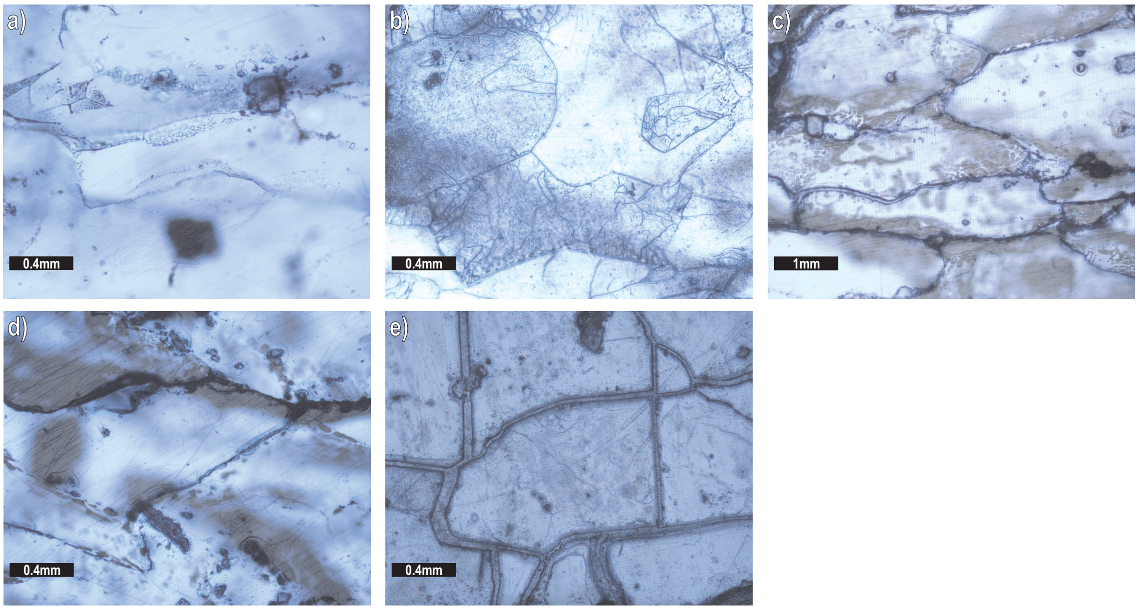

Figure 8. *Microphotographs from the rock salt. For description of recorded microstructure see the text in the section 6. Note different scale of image c).*

Microstructural description and analysis were carried out from salt thin sections cut parallel to the k1k3 plane of the AMS core samples, namely the 1a, 3a and 4a from the SE, and 22, 24, and 26a from the NW dyke aureole. The digitization of microstructures was carried out from mosaics of micrographs in the ESRI ArcMap® GIS environment, and further processed using the MATLAB® PolyLX Toolbox (Lexa et al., 2005; http://petrol.natur.cuni.cz/~ondro/polylx:home). The grain size (equal area diameter), the axial ratio and the shape preferred orientation of traced salt grains and solid inclusions, and size of salt subgrains were quantified. The shape preferred orientation (SPO)

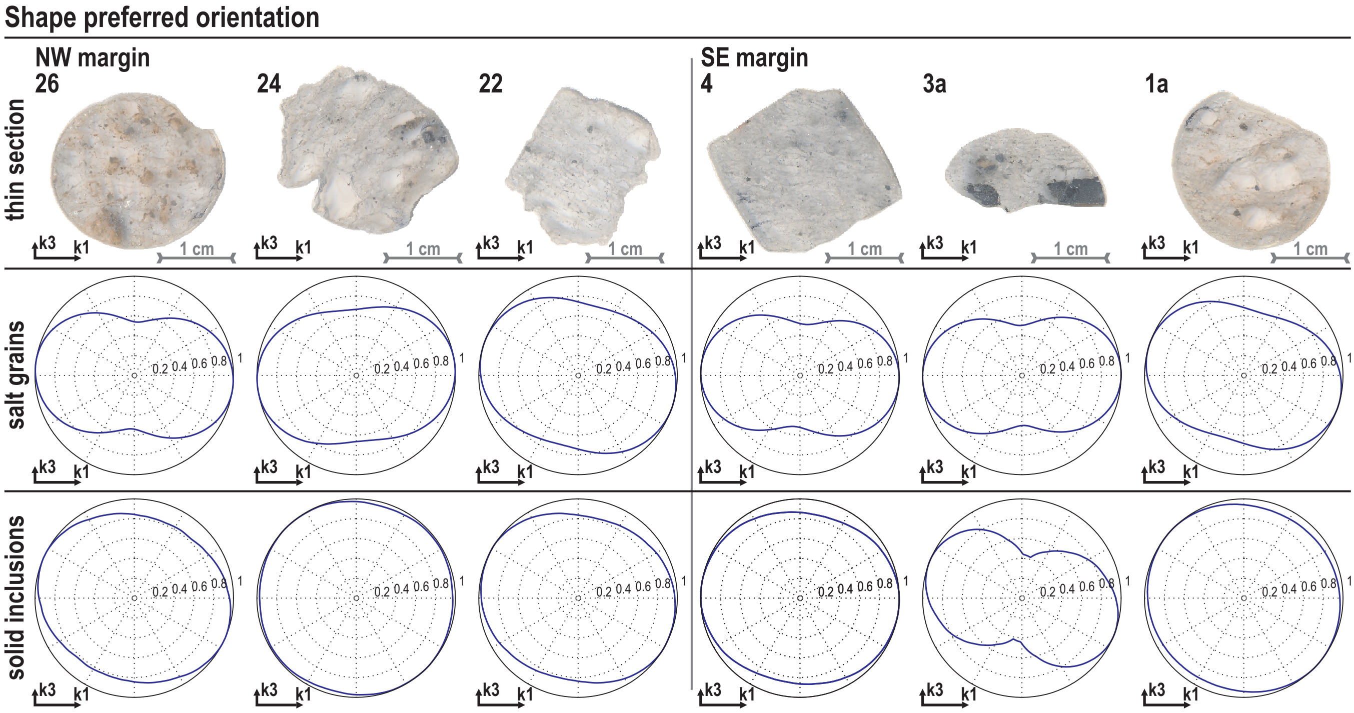

Figure 9. *The results of the shape preferred orientation (SPO). First row shows the photographs of the selected thin sections. The second row illustrates the orientation of the salt grains and the third row shows the SPO of solid inclusions. The k_1 and k_3 axis orientations are shown next to each diagram.*

of salt grains and solid inclusions was determined using the PAROR method (Panozzo, 1983, 1984). The long and short axes of the individual grains were derived, and diagrams representing the orientation distribution functions of grains long axes were plotted in the graph in Fig. 9.

Solid inclusions collected from the distal part of the dyke aureole consist mainly of anhydrite, minor quartz and clay minerals that all mark halite grain boundaries. Only at the SE dyke contact, solid inclusions are represented by angular dyke fragments up to 15 mm in diameter. Distal parts of the dyke aureole (2.5 m from NW dyke wall, and 0.75 m from SE dyke wall), show microstructures rich in salt porphyroclasts up to 10 mm in length (Fig. 8a, b, 9), frequently consumed by new (substructure-free) grains. With decreasing distance to the dyke contact, halite grains are relatively more elongated, the porphyroclasts decrease in amount and size, and finally disappear completely close to the dyke margin. Fibrous and slightly bent halite grains formed at the edges of dyke fragments at the SE margin of the dyke. Such grains form the “pressure fringe” grain aggregates in the stress shadows of porphyroclasts (e.g. Cox and Etheridge, 1983; Paschier and Trouw, 2005). Unspecified precipitates mark the grain boundaries of relatively equigranular halite grains close to both dyke margins (Fig. 8c-e). At the SE margin of the dyke, these veins locally crosscut the halite grains at angles of 45° to the shape preferred orientation of the halite grains. In contrast, at the NW margin of the dyke, halite shows a polygonal mosaic of grain boundaries where the unspecified precipitates form an almost continuous inter- and intra- granular network with individual segments up to 100 µm thick (Fig. 8e), which resembles a “dilated aggregate” where fluids penetrate deforming aggregates at low effective pressures (Urai et al., 2008).

The grain size (equal area diameter) and axial ratio of salt grains exhibit lognormal distribution, and their median values range in all specimens from 0.38 to 0.86 mm and from 1.73 to 2.24, respectively (Table 1). The median grain size shows a subtle increase towards the dyke contact (Table 1). Both types of solid inclusions have median value of grain size (0.10 to 0.27 mm) as well as axial ratio (1.38 to 1.98) lower than salt grains. The subgrain size piezometry (Table 1) suggests values of the resolved differential stresses similar for both SE and NW dyke aureoles, and a clearly increasing trend towards the NW side of the dyke, from 1.96 to 2.85 MPa, with a maximum value of 3.93 MPa at 30 cm from the dyke SE margin, which is enriched in angular dyke fragments.

Table 1 Results of quantitative microstructural analysis

Sample		**EAD [mm]**				**AR []**				**subgrains EAD [μm]**				**Diff.**
		max	min	mean	median	max	min	mean	median	max	min	mean	median	**stress[Mpa]**
1a	*salt*	5.70	0.01	0.50	0.43	5.00	1.01	1.99	1.84	189.12	19.49	76.81	70.54	2.64
	solid incl.	0.50	0.04	0.10	0.10	3.69	1.00	1.46	1.38					
3a	*salt*	1.96	0.04	0.44	0.36	7.35	1.00	2.35	2.12	206.08	12.06	51.17	44.60	3.93
	solid incl.	26.64	0.02	0.30	0.12	7.51	1.00	1.74	1.54					
4a	*salt*	3.70	0.12	0.73	0.66	6.12	1.01	2.30	2.15	334.43	18.48	103.13	91.26	2.11
	solid incl.	0.70	0.07	0.21	0.18	3.19	1.00	1.70	1.62					
22	*salt*	4.07	0.01	0.68	0.59	12.68	1.02	1.93	1.73	370.37	22.59	77.32	64.59	2.85
	solid incl.	0.57	0.06	0.22	0.18	3.02	1.02	1.64	1.43					
24	*salt*	9.97	0.26	1.06	0.86	6.09	1.01	2.07	1.90	292.84	4.46	112.79	96.12	2.02
	solid incl.	1.27	0.06	0.17	0.14	3.30	1.04	1.45	1.40					
26a	*salt*	3.01	0.08	0.72	0.61	6.99	1.05	2.36	2.24	379.41	33.52	113.31	99.21	1.96
	solid incl.	1.71	0.09	0.41	0.25	4.21	1.05	1.97	1.84					
BL	*salt*	3.24	0.00	0.45	0.38	8.58	1.01	2.33	2.07	626.13	43.13	154.20	127.02	1.58
	solid incl.	2.80	0.08	0.43	0.27	7.30	1.04	2.21	1.98					

Equal area diameter (EAD), axial ratio (AR), calculated differential stress based on EAD of subgrains.

In all specimens, the SPO of both salt grains and solid inclusions is subparallel to the maximum magnetic susceptibility axis (k_1), with significantly stronger degree of SPO for the salt grains. The only exception from this correlation is found for sample 3a (SE margin), where the dyke fragments are strongly aligned and their SPO shows an angular difference of about 20° from the main SPO of salt grains.

7 Crystallographic preferred orientation

The crystallographic preferred orientation (CPO) of halite crystal aggregates was established by means of electron back-scattered diffraction (EBSD) in order to document, together with results of the microstructural analysis, the deformation mechanisms of fabric formation in rock salt adjacent to the lamprophyre dyke. The EBSD data were acquired at an accelerating voltage of 20 keV, a 39 mm working distance, and a ~5 nA beam current using NORDLYS II (HKL Technology) EBSD system mounted on the TESCAN Vega scanning electron microscope in the mapping mode with 10 μm step size at Institute of Petrology and Structural Geology of the Faculty of Science at Charles University in Prague. In all specimens, several maps were acquired and then merged in CHANNEL5 software. The EBSD maps were processed, grain and subgrain boundaries were drawn, and pole figures were plotted using MATLAB® Toolbox for Quantitative

Texture Analysis (MTEX) (Bachmann et al., 2010; 2011; https://code.google.com/p/mtex/) and are presented in Fig. 10 and stored at PANGEA (http://doi.pangaea.de/10.1594/PANGAEA.820353?format=html). A misorientation value > 0.5° was used for subgrain detection, and a misorientation > 5° was used to recognize grain boundaries. A similar result was observed after replotting the grain boundary topology for misorientation > 10°. The CPO is presented in contoured pole figures of one measurement per grain with misorientation > 5°.

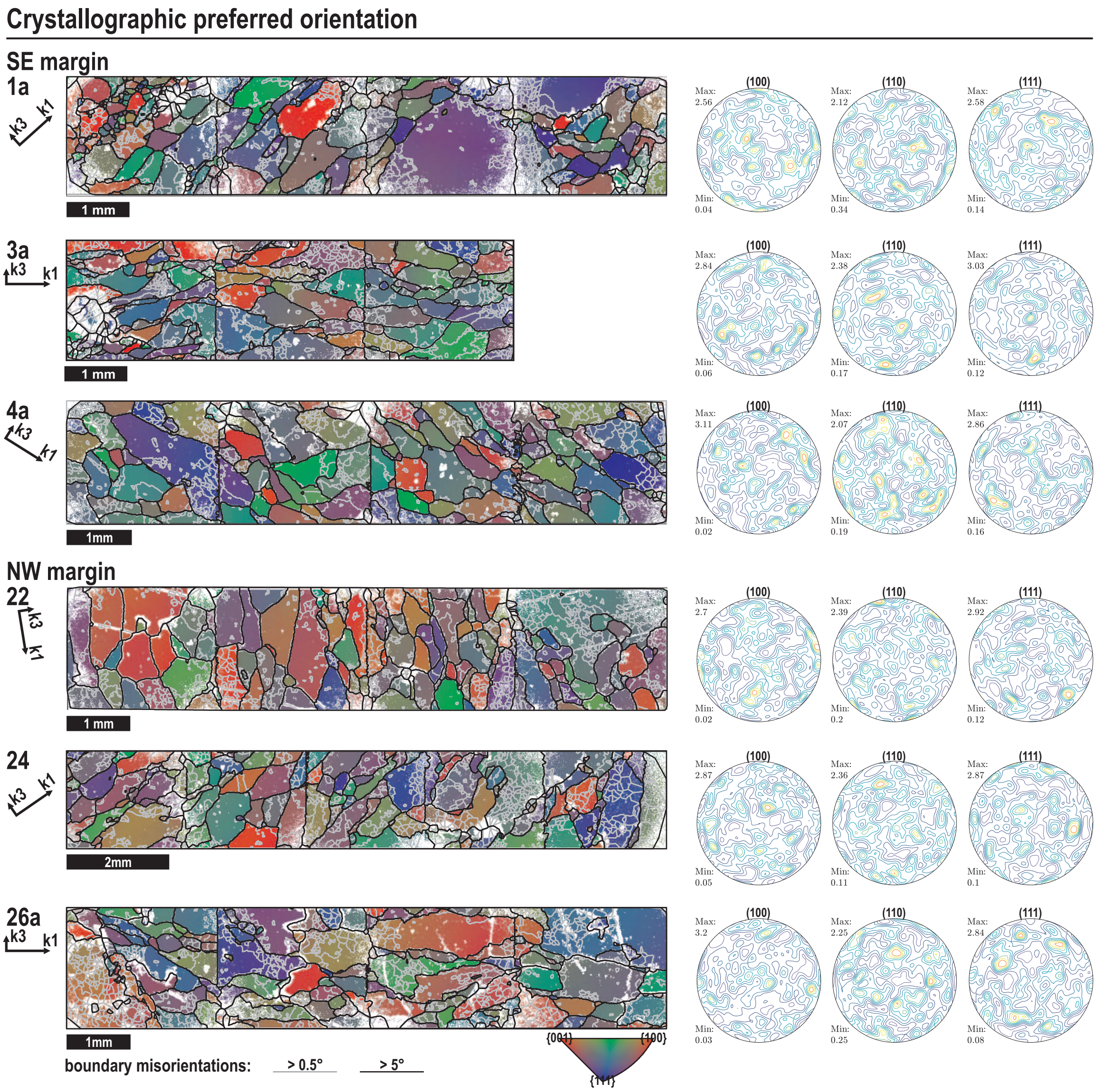

Figure 10. Results of the crystallographic preferred orientation (CPO) obtained by the electron back-scattered imaging (EBSD) method. The CPO is measured for both margins NE and SE and is presented in terms of CPO maps and on lower hemisphere pole figures. The CPO maps are colored based on inverse pole figure of maps long edge orientation.

The mapping of the CPO confirms the presence of subgrains in all specimens and an increasing number of grains lacking low angle misorientation substructures with decreasing distance from dyke (Fig. 10). The EBSD measurements reveal very weak CPO for all samples, almost random.

EBSD maps and the CPO suggest that several deformation mechanisms operated simultaneously in the rock salt to form both the primary fabric far from the dyke and the secondary fabric near the dyke margins. Distant from the dyke, the primary fabric has formed by deformation with important role of dislocation creep regime, as documented by the large number of subgrains and core and mantle microstructure in porphyroclasts of sample 1a. Towards both dyke margins, the increasing number of subgrain free halite grains and random CPO suggests the combined effects of diffusion driven fluid assisted grain boundary migration and solution-precipitation creep. Nevertheless, these deformation mechanisms were also accompanied by dislocation creep, documented by subgrains in highly elongated halite grains.

8 Heat transfer modelling

Thermal mathematical modelling of the temperature field outside and inside the dyke was carried out to consider the mode of host rock deformation in terms of solid-state deformation mechanisms and mobility of fluids, and to determine if the heat transfer was sufficient to melt the host rock salt. A two-dimensional thermal model of a 3 m wide vertical dyke intruded in halite was created to study the possible temperature distribution immediately after dyke emplacement. The thermal model was constructed using the Comsol and Fracture software (Kohl and Hopkirk, 1995), and includes a hypothetical initial temperature of the intrusion of 1400 °C, and temperature of host rock salt of 35 °C at the depth of 1 km for contemporaneous heat flow of 70 mW/m^2 and mean annual surface air temperature in the study region in the range 20–25 °C. However it can be assumed that the background heat flow from the lower portions of the crust was higher at the time of emplacement of the lamprophyre dyke, therefore temperature of host rock salt was at 35 °C, which corresponds to heat flow of 120 mW/m^2. The model includes latent heat of basalt (400 KJ/kg), which is dissipated in the temperature range of 750–1100 °C. The dependence of thermal conductivity on temperature is also included. The latter is remarkable especially for halite (6 W/mK at 0 °C and ca. 1.5 W/mK at 800°C). The melting temperature of halite is ca. 801 °C. The material thermophysical parameters at 20 °C are the following: 1) density 2700 kgm^{-3} for the lamprophyre, and 2165 kgm^{-3} for the rock salt; 2) thermal capacity of 1000 Jkg^{-1}K^{-1} for the lamprophyre, and 855 Jkg^{-1}K^{-1} for the rock salt; 3) thermal conductivity of 6 Wm^{-1}K^{-1} for the lamprophyre, and 1.5 Wm^{-1}K^{-1} for the rock salt.

The modelling results suggest that, for the used set of parameters, the rock salt in the vicinity of the 3 m thick lamprophyre dyke should not melt. This is supported by curves of temperature distribution at 10 hours intervals after the emplacement (Fig. 11a). The inflexion point of all these curves at the contact between both lithologies clearly indicates that the maximum temperature reached in the host salt never exceeded 650 °C. The maximum temperature in the host rock salt rapidly decreases with distance from the contact, reaching less than 250 ºC at 1 m from the contact, as exemplified in Fig. 11b.

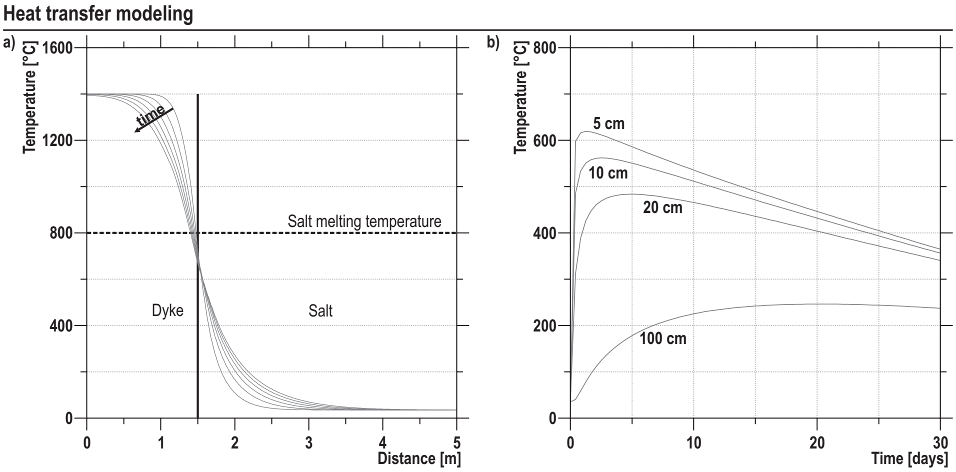

Figure 11. *Results of the thermal modelling. a) Distribution of the temperature at 10 hours intervals after the emplacement; b) The temperature in salt host rock at variable distance from the contact. For more details, see the text.*

9 Discussion

9.1 Magnetic fabric

The AMS fabric in the dyke is carried by multidomain ferrimagnetic minerals, most likely magnetite, as documented by the thermomagnetic and hysteresis analyses (Fig. 2e-g, 3, 4). The AMS fabrics (Fig. 6a) revealed a NE-SW foliation on both margins, dipping at the NW side about 80º towards the core of the dyke. The magnetic lineation is subvertical at both margins. The vertical dyke-parallel planar fabric away from dyke margins is in agreement with “normal magnetic fabric” reflecting magma flow as described by Rochette et al. (1991) for basaltic dykes from the Oman ophiolite. The observed imbrication between magnetic foliation and dyke plane close to the dyke margins can be attributed to the flow effect along dyke margins. It seems to indicate a downward flow but there is a problem in interpreting the direction of flow as far as we have signs of rotation and cannot be sure about the original position. Moreover, Silva et al. (this issue) argue that this type of fabric does not necessarily reflect the magma flow.

In the centre of the dyke, the magnetic foliation remains subvertical, but its strike is perpendicular to the dyke walls and bears a subhorizontal lineation. The centre of the dyke is also characterized by increased magnetic susceptibility. The vertical magnetic foliation bearing horizontal lineations perpendicular to dyke plane is similar to the reverse fabric described by Rochette et al. (1991), and one of the type of fabrics (IIb) described by Raposo and Ernesto (1995) in the Ponta Grossa dyke swarm in Brazil. These authors explained such fabric as resulting from magma under stress in extension. A similar fabric orientation was also described by Kratinová et al. (2010) and Kusbach (2007) in non-scaled analogue models of a sheet-like or tabular vertical intrusion constrained by a planar discontinuity that was continuously opening in front of an advancing intrusion. They explained the fabric by lateral expansion of the tabular body. However, it is important to notice the incomplete girdle distribution of k_3 axes, which could point also to the presence of a composite fabric (Henry, 1997). In addition, the increase of k_3 plunge corresponds to T values changing from oblate to neutral ellipsoids. A similar pattern was identified by Silva et al. (2008) as a signature of composite fabrics.

The AMS measurements in the rock salt (Fig. 6b) reveal a transition of the magnetic fabric with decreasing distance from the dyke. The magnetic fabric changes from an overall regional pattern (mainly characterized by magnetic foliations steeply dipping towards NE, and lineations scattered along the mean foliation plane) to a dyke–related fabric (magnetic foliation subparallel to the NE-SW subvertical dyke, and subvertical lineations). The magnetic mineralogy study on the rock salt shows the combined role of dia-, para- and ferrimagnetic minerals of prevailing multidomain character, documented by thermomagnetic and hysteresis analyses (Figs. 2a-c, 3, 4). The interpretation of the asymmetric AMS fabric pattern in terms of magnetic foliation orientation and magnetic susceptibility values on the opposite dyke walls is complicated by the fact that the AMS data are not statistically well representative, and are of low susceptibility at the NW margin. Whereas a progressive change of the dip angle for the NE-SW trending planar fabric from about 75° (to the SE) to the vertical orientation is recorded at the NW wall of the dyke, the planar fabrics at the opposite (SE) wall of the dyke rotate rather abruptly. The more scattered orientation of the magnetic foliation on the SE side can be attributed to the presence of relatively large angular dyke fragments, which gives a composite character of the fabric. The mean magnetic susceptibility oscillates around zero in the rock salt at the NW wall of the dyke, which is in agreement with the values obtained for salt specimens representing the regional AMS fabric recorded in the mine. On the SE side of the dyke, the mean magnetic susceptibility of rock salt samples increases towards the dyke margin, from values around zero (corresponding to samples where the regional AMS fabric is preserved) to values of 445×10^{-6} SI next to the margin (where the AMS fabric is dyke-related). The recorded increase in magnetic susceptibility correlates with the increasing amount of angular dyke fragments (exhibiting a magnetite type of thermomagnetic behaviour) in the rock matrix.

9.2 Relationship between magnetic and rock fabrics

To assess the relevance of the obtained AMS fabric to the rock salt texture, a quantitative microstructural analysis study of halite grains and solid inclusions was performed (Fig. 9). Two types of solid inclusions were observed in the rock salt. One type occurs in all specimens originated during deposition of the rock salt (anhydrite, minor quartz and clay minerals). The other type of solid inclusions, only observed at the SE side of the lamprophyre dyke, is described as lamprophyre rock fragments of angular shape. The volume of such solid inclusions increases in specimens collected closer to the SE dyke margin (Table 1). The microstructural analysis of halite grains as well as solid inclusions in sections parallel to k_1 and k_3 principal susceptibility axes exhibits shape preferred orientations more or less perpendicular to k_3 and parallel to k_1 (Fig. 9). This observation shows that AMS describes correctly the orientation of the rock fabric, even in very low magnetic susceptibility rocks like salt. However, the quantitative interpretation of the AMS fabric (in terms of shape and intensity values) is limited due to low values of magnetic susceptibility in the rock salt, within the range of values close to zero, where the strength of AMS cannot be interpreted (Hrouda, 2004; 1986).

9.3 Paleomagnetic analysis

Nine coherent paleomagnetic data have been obtained within the dyke (D = 81.2º, I = 22.6º, k = 321 and α_{95} = 2.9º) (Fig. 7). This direction is very far from those obtained in rocks of similar age in the same area, at Monchique (D = 182º, I = 37º, Van der Voo, 1969; D = 181º, I = 42º, Storetvedt et al., 1990) and Sines (D = 1.5º / I = 42.3º, Ribeiro et al., 2013). The present orientation of the dyke is therefore very different from that during its emplacement. That agrees well with the supposed diapiric ascent of the salt body after dyke intrusion (Terrinha et al., 1994 and Terrinha, 1989). The few paleomagnetic data (D = 78.3º, I = 25.7° and D = 267.7º, I = 12.7º) obtained for rock salt with abundant lamprophyre fragments have different paleomagnetic directions from those of the dyke itself. Therefore the structural evolution recorded in the rock salt is more complicated than in the lamprophyre dyke.

9.4 Microstructural analysis

The results of quantitative microstructural analysis in the rock salt suggest a progressive change in the texture of rock salt aggregates with decreasing distance to the lamprophyre dyke (Fig. 12). Towards the dyke, the main textural trends are as follows: (1) the amount and size of sigmoidal halite porphyroclasts decrease; (2) the size of subgrains together with their abundance decreases as shown by the CPO maps (Fig. 10); (3) there is an increase in the amount and thickness of inter-granular precipitates surrounding and locally cross-cutting individual halite grains in dilated halite aggregates (Fig. 8e); (4) the median halite grain size increases (Table 1), except for specimens 3a and 22. While in specimen 3a grain size growth was likely inhibited by the presence of angular lamprophyre fragments, for specimen 22 the grain size was probably underestimated due to intra-granular microcracks, which could be confused with grain boundaries during digitization. The axial ratio of halite grains also increases (Table 1), although an opposite trend was recorded in the NW dyke wall, where it can be attributed to grain crack splitting.

The described microstructures are compatible with simultaneous fluid-assisted dislocation creep and solution-precipitation creep during development of the dyke-parallel fabric (Pennock et al., 2005, 2006a,b; Schléder and Urai 2007; Schléder et al., 2007; Ter Heege et al., 2005a,b; Trimby et al., 2000; Urai et al., 2008; Urai et al., 1987). The dislocation creep mechanism operating inside the grains is documented by observed substructures in the halite grains. Clear (substructure-poor) grains invading the substructure-rich grains with lobate grain boundary segments point to fluid assisted grain boundary migration (GBM) associated with solution-precipitation transfer across the grain boundaries. On the other hand, the random CPO (Fig. 10), straight grain boundaries, highly elongated grains lacking substructures, and the presence of precipitates on grain boundaries (Fig. 8, 12) can be associated with grain boundary sliding (GBS) combined with solution-precipitation (SP) creep transferring mass along grain boundaries (Urai et al., 2008, Závada et al., 2012). More equilibrated equigranular textures of relatively elongated grains with random CPO, and the presence of precipitates in the halite microstucture formed at the dyke contacts at the expense of porphyroclasts (Fig. 9, 12). This would be compatible with decreasing differential stress conditions during flow and/or increased availability of an interstitial fluid phase towards the dyke contact. In contrast, decreasing subgrain size towards the NW side of the dyke wall suggests that the differential stress increased towards the dyke walls (Table 1). Relatively large recorded differential stresses for specimen 3a in the SE wall of the dyke are attributed to the large lamprophyre rock fragments that could produce local stress concentrations at their edges during deformation.

In summary, the microstructural evolution suggests an increasing influence of the diffusion driven deformation mechanisms towards the contacts with the dyke at increased differential stresses. That is also compatible with the dilatancy coupled with intragranular microcracking that becomes another important strain accumulation process (Renner, 2000; Urai, 1986; Urai et al., 2008). The temperature increase at solution-precipitation creep conditions elevates the diffusion rate, and thus reduces the flow strength and increases the strain rate, as deduced from published flow laws of solution-precipitation creep (Ter Heege et al., 2005a; Urai et al., 2008). Similarly, the presence of water in the microstructure of the salt polycrystalline aggregates facilitates the diffusion controlled deformation mechanisms, again reducing significantly the flow strength of the salt (Peach et al., 2001; Ter Heege et al., 2005b). Therefore, the increase of temperature and/or water content would explain the increasing dominance of fluid assisted grain boundary migration and solution-precipitation creep and dilatancy, coupled with increasing differential stress at constant grain size towards the dyke margin. The lack of microstructures indicating crystallization of salt from melt (e.g. rectangular substructure-free grains) near the dyke is in agreement with temperature conditions predicted by the thermal modelling of heat transfer between dyke and host rock salt (Fig. 11, 12). The dilatancy behaviour of the microstructure at high fluid activity often results in ‘‘dilation hardening’’, rendering the rock stronger and likely much less deformable than the surrounding non-dilated equivalent (Renner et al., 2000; Závada et al., 2007).

We assume that the magma ascent and emplacement resulted in the development of a microstructural gradient in the salt towards the dyke contacts (Fig. 12), and that the dilated halite aggregates host precipitated fluid phase derived from an external reservoir in the aureole of the advancing hot intrusion. The concomitant superposed gradients of water availability, differential stress and temperature adjacent to the dyke, represent an interesting field of physical conditions with significant implications for example regarding basins with high heat flow.

9.5 Structural interpretation

To determine the origin of the structural pattern acquired by the salt in the vicinity of the lamprophyre dyke, a link has to be made between data and interpretations from all the applied methods.

The AMS and magnetic studies provided trends of fabric in both igneous and salt rocks. The AMS fabric across the lamprohyre dyke, together with the magmatic texture without any sub-solidus deformation overprint, suggests that the primary emplacement-related fabric was not affected by later deformation. In the salt, there is a change in the fabric orientation, from regionally recorded NW-SE trending steep foliation to NE-SW subvertical dyke parallel foliation closer to the dyke (Fig. 12). The quantitative microstructural analysis confirmed that AMS in this case correctly describes the orientation of the rock fabric in the salt (Fig. 9). However, to decipher the processes that led to the formation of the dyke-parallel planar fabric, more detailed study of rock salt microstructure and texture were necessary. They revealed that, with decreasing distance from the dyke, unusual microstructural changes occurred in the salt (Fig. 12), characterized by high temperature, high fluid activity, random CPO but also high stress (see section 9.4). However, the thermal modelling surprisingly showed that the salt

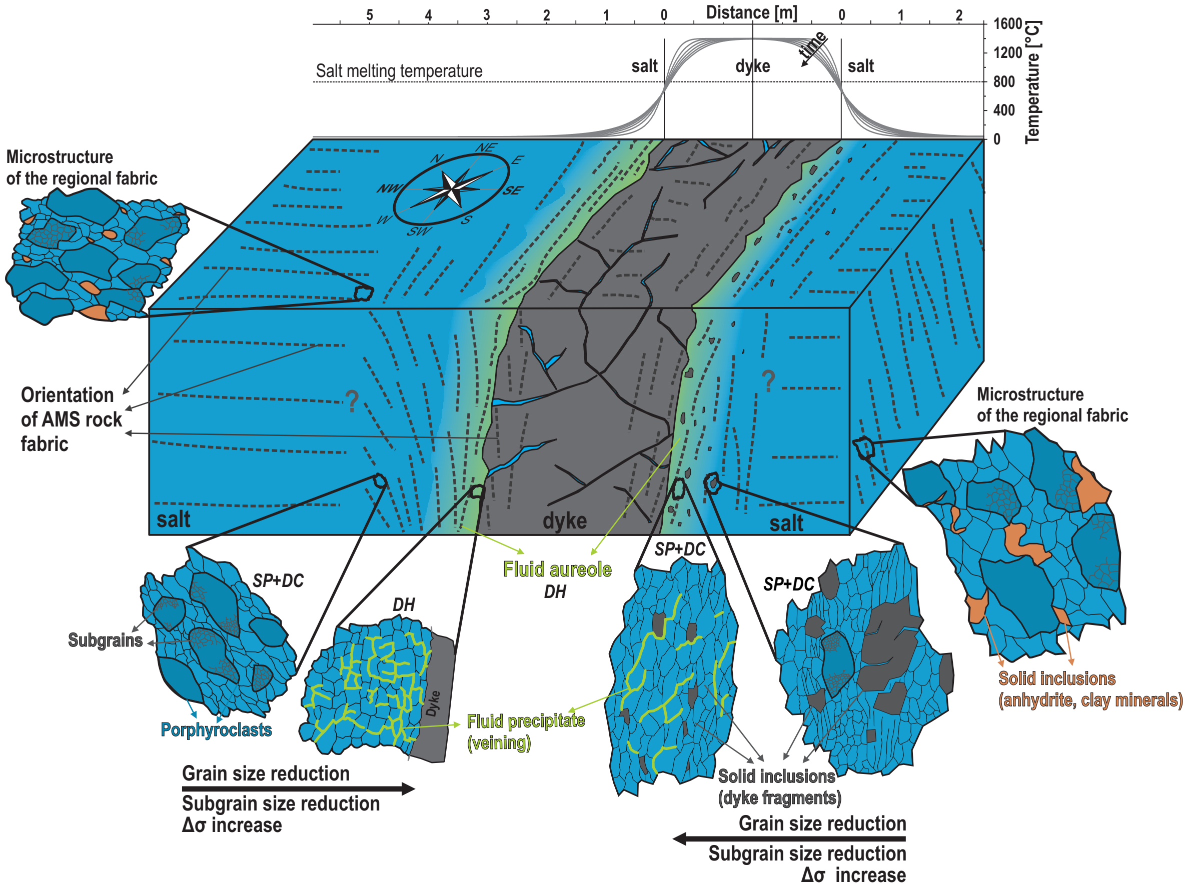

Figure 12. *Block diagram ilustrating the most important findings and interpretations of AMS, microstructural analysis and thermal modelling. Operating deformation mechanisms: SP+DC - solution precipitation + dislocation creep, DH - Fluid overpressure driven dilation hardening. $\Delta\sigma$ - differential stress. The geographic orientation of the block diagram is marked by the compass rose.*

should not melt even at the salt/dyke contact. Paleomagnetic results evidenced that dyke has rotated from its original position, and thus additional deformation affected the dyke/salt system.

The structural record can by ascribed to three different deformational events. The coarse grained regional fabric is most probably related to the diapiric upward flow of the salt body. The dyke-parallel planar fabric at the NW side is assumed to be related to the dyke intrusion keeping the dyke emplacement- or ascent-related fabric likely due to the stress-shadow effect around the rigid dyke (Passchier and Trouw, 2005). However, the asymmetrical fabric patterns on the opposite sides of the dyke, together with the apparent rotation of angular lamprophyre fragments, indicate a tectonic reworking of the dyke-parallel planar fabric at the SE side of the dyke. Taking into account also the character of the dyke-salt contact, the SE margin appears to be modified by tectonic-related deformation overprinting the dyke emplacement-related fabric. However, we can not exclude the possibility that angular fragments in the rock salt originated as peperite breccia during the first contact of lamprophyre magma with cold and wet salt, and not during deformation after dyke emplacement. Therefore it is possible that the structure on both sides of the dyke originated due to dyke emplacement.

The origin of the observed individual fabrics described above is difficult to interpret in terms of fabric superposition and relationship with the tectonic events that are found in the Algarve basin (Terrinha, 1998), unless a detailed AMS and microstructural study is carried out for the whole Loulé diapir. Therefore, based on the AMS and rock salt microstructure, two tectonic and rather speculative scenarios are suggested: (1) In the first one, the vertical NW-SE trending regional planar fabric in the salt originated during the diapiric ascent because the diapirism was likely reworking most of the rock salt mass during the upward flow. Later intrusion of the dyke produced a dyke-parallel planar fabric in the host rock salt that is preserved along the NW side of the dyke. This is documented by the progressive evolution of the microstructure towards the dyke, from coarse-grained porphyroclastic to the equilibrated finer-grained microstructure, with elongated grains. Finally, a localized shear zone developed at the SE dyke-salt contact during the regional Tertiary to Quaternary deformation phase (Terrinha, 1998), probably because of the favourable orientation of the dyke-salt interface for slip with respect to the regional stress field. This scenario should imply that the diapirism took place before the dyke intrusion dated at ~72 Ma (Miranda et al., 2009), and that is in contradiction with the diapirism timing suggested by Terrinha et al. (1990, 1994). (2) The second scenario begins with intrusion of the dyke and development of the dyke-parallel planar fabric. Then the diapiric ascent of the salt induces the localized tectonic fabric along the SE side of the dyke. The NW side should have been partly shielded by the rigid dyke from the tectonic reworking to retain the microstructural evolution acquired during dyke intrusion. Finally, the Tertiary-Quaternary tectonics resulted in the regional fabric in the salt farther from the dyke.

It is important to underline that both scenarios have similar interpretation concerning the microstructural observation of progressive fabric evolution along the NW side. The “transition zone” with progressive orientation change of the salt foliation results mainly from the superposition of two events (diapir ascent followed by intrusion for the first scenario, and intrusion followed by diapir ascent for the second one) and its fabric is therefore in both cases composite. Another common fact is that the rigid dyke “protected” its NW side from plastic deformation that affected the rock salt far from the dyke.

10 Conclusion

The studied rock salt-dyke zone represents a remarkable example of contact of rocks with very different physical characteristics, expressed as petrographic, mechanic, calorimetric and magnetic properties. The fabrics of both lamprophyre and rock salt record magmatic intrusion, “plastic” flow and regional deformation.

The AMS study in the lamprophyre dyke revealed the fabric related to the emplacement of magma with lateral expansion of the tabular body or extension along dyke strike. In the rock salt, two contrasting AMS fabrics associated with different rock salt microstructures have been recognized: the coarse-grained rock salt with steeply dipping NW-SE striking regional planar fabric, and the NE-SW subvertical planar fabric parallel to the dyke in its close vicinity. The quantitative microstructural analysis of halite texture and solid inclusions confirmed that AMS is capable of describing correctly the orientation of the fabric in the rock salt. The gradients in microstructructural characteristics are attributed to salt deformation related to dyke emplacement. However, the reveald asymmetry in salt microstructure on opposite sides of the dyke suggests that the SE margin of the dyke was modified by subsequent tectonic-related deformation. The NW side seems to have kept the dyke intrusion-related salt fabric (protected by the rigid dyke). The paleomagnetic data obtained on the lamprophyre dyke shows values very far from those obtained in rocks of similar emplacement age in the area. This documents very strong rotation of the whole dyke during latter tectonic events.

Acknowledgements

We thank Alexandre Andrade and Mina Campina de Cima, Quimigal SA, who permitted to carry out work in the mine and was of great assistance during structural work and sample collection. We are also indebted to Martin Racek for his selfless assistance with EBSD measurements. We are grateful to two anonymous reviewers and the editor for helpful and constructive reviews which improved the manuscript. This work was funded by a Portuguese scientific grant No.: PTDC/CTE-GIX/098696/2008 (Pedro Silva) and from institutional support to the Institute of Geophysics, Academy of Sciences of the Czech Republic (RVO 67985530).

The AMS data and EBSD maps of the salt-dyke contact zone are archived in the PANGAEA database at the Alfred Wegener Institute for Polar and Marine Research (http://doi.pangaea.de/10.1594/PANGAEA.820353?format=html).

References

- *Ade-Hall, J.M., Palmer, H.C, Hubbard, T.P., 1971. The magnetic and opaque petrological response of basalts to regional hydrothermal alteration. Geophys. J. R. astr. Soc. 24, 137 – 174. Baer, G., 1991. Mechanisms of dyke propagation in layered rocks and in massive, porous sedimentary rocks. J. Geophys. Res., 96, 11911 – 11929.*

- *Bachmann, F., Hielscher, R., Schaeben, H., 2010. Texture Analysis with MTEX - Free and Open Source Software Toolbox, Sol. St. Phen. 160, 63 – 68.*

- *Bachmann, F., Hielscher, R., Schaeben, H., 2011. Grain detection from 2d and 3d EBSD data - Specification of the MTEX algorithm. Ultramicroscopy 111, 1720 – 1733.*

- *Borges, M.E.N., Riding, J.B., Fernandes, P., Matos, V., Pereira, Z. 2012. Callovian (Middle Jurassic) dinoflagellate cysts from the Algarve Basin, southern Portugal. Rev. Palaeobot. Palyno. 170, 40 – 56.*

- *Borradaile, G. J., and Henry, B., 1997. Tectonic applications of magnetic susceptibility and its anisotropy. Earth Sci. Rev. 42, 49 – 93. Borradaile, G. J., and Jackson M., 2010. Structural geology, petrofabrics and magnetic fabrics (AMS, AARM, AIRM). J. Struct. Geol. 32(10), 1519 – 1551.*

- *Chadima M., and Jelínek V., 2008. Anisoft 4.2. – Anisotropy Data Browser. Paleo, Rock And Environmental Magnetism 11th Castle Meeting. Contributions to Geophysics and Geodesy. 38, 41.*

- *Correa-Gomes, L.C., Souza Filho, C.R., Martins, C.J.F.N., Oliveira, E.P. 2001. Development of symmetrical and asymmetrical fabrics in sheet like igneous bodies: the role of magma flow and wall-rock displacements in theoretical and natural cases. J. Struct. Geol. 23, 1415 – 1428.*

- *Cox, S.F., and Etheridge, M.A., 1983. Crack-seal fibre growth mechanisms and their significance in the development of oriented layer silicate microstructures.Tectonophysics 92, 147 – 170.*

- *Day, R., Fuller, M., Schmidt, V.A., 1977. Hysteresis properties of titanomagnetites: grain size and compositional dependence. Phys. Earth Planet. Interiors 13, 260 – 267.*
- *Desbois, G., Závada, P., Schléder, Z. and Urai, J. L., 2010. Deformation and recrystallization mechanisms in actively extruding salt fountain: Microstructural evidence for a switch in deformation mechanisms with increased availability of meteoric water and decreased grain size (Qum Kuh, central Iran), J. Struct. Geol. 32(4), 580 – 594.*
- *Dunlop, D.J., 2002. Theory and application of the Day plot (Mrs/Ms versus Hcr/Hc). 1. Theoretical curves and tests using titanomagnetite data. J. Geophys. Res. 107 (B3).*
- *Dunlop, D.J., Özdemir, Ö.,1997. Rock Magnetism: fundamentals and frontiers. Cambridge Studies in Magnetism Cambridge University Press, pp 573.*
- *Fisher, R.A. 1953. Dispersion on a sphere. P. Roy. Soc. A, 217, 98 – 102.*
- *Henry, B. 1997. The magnetic zone axis: A new element of magnetic fabric for the interpretation of the magnetic lineation. Tectonophysics 271, 325 – 329.*
- *Hrouda, F., 1982. Magnetic anisotropy of rocks and its application in geology and geophysics. Geophys. Surv. 5, 37 – 82.*
- *Hrouda, F., 1986. The effect of quartz on the magnetic anisotropy of quartzite. Stud. Geophys. Geod. 30 (1), 39 – 45.*
- *Hrouda, F., 1994. A technique for the measurement of thermal changes of magnetic susceptibility of weakly magnetic rocks by the CS-2 apparatus and KLY-2 Kappabridge. Geophys. J. Int. 118, 604 – 612.*
- *Hrouda, F., 2004. Problems in interpreting AMS parameters in diamagnetic rocks, in: Martin-Hernandez, F., Luneburg, C., Aubourg, C., Jackson, M. (Eds.), Magnetic Fabric: Methods and Applications, Geo. Soc. Spec. Pub. 238, London, 49 – 59.*
- *Hrouda, F., Jelínek, V., Hrušková, L., 1990. A package of programs for statistical evaluation of magnetic data using IBM-PC computers. AGU 1990 fall meeting. Eos, Transactions, American Geophysical Union 71, pp. 1289.*
- *Hrouda, F.; Šmíd, J.; Schulmann, K., 2001. Anisotropy of magnetic susceptibility and its carriers in salt domes of the SW Zagros Mts. Iran. Amer. Geophys. Un., Fall Meet. abstract GP41A-0247.*
- *Jelinek, V., 1978. Statistical processing of magnetic susceptibility measured in groups of specimens. Stud. Geophys. Geod. 22, 50 – 62.*
- *Jelinek, V., 1981. Characterization of the magnetic fabric of rocks. Tectonophysics, 79, 63 – 67.*
- *Jelínek, V., and Pokorný, J., 1997. Some new concepts in technology of transformer bridges for measuring susceptibility anisotropy of rocks. Phys. Chem. Earth. 22, 179 – 181.*
- *Kirschvink, J.L., 1980. The least-squares line and plane and the analysis of palaeomagnetic data. Geophys. J. Roy. astr. Soc. 62, 699 – 718.*
- *Knipping, B., 1989. Basalt Intrusions in Evaporites. Lecture Notes in Earth Sciences. Springer-Verlag, pp 138.*
- *Kohl, T., and Hopkirk, R.J., 1995. Fracture – a simulation code for forced fluid-flow and transport in fractured, porous rock. Geothermics 24(3), 333 – 343.*
- *Kratinová, Z., Machek M., Kusbach V., 2010. Fabric transpositions in granite plutons - an insight from non-scaled analogue modeling, J. Geol. Soc. India 75, 267 – 277.*

- *Kusbach V., 2007. Analogue modeling of fabric development in dome shaped volcanic bodies. MSc Thesis, Prague, Charles University.*
- *Lexa, O., Štípská, P., Schulmann, K., Baratoux, L., Kröner, A., 2005. Contrasting textural record of two distinct metamorphic events of similar P-T conditions and different durations. J. Metamorph. Geol. 23 (8), 649 – 666.*
- *Marques, F.O., Burg, J.-P., Armann, M., Martinho, E., 2013. Rheology of synthetic polycrystalline halite in torsion. Tectonophysics 583, 124 – 130.*
- *Martins, L.T., 1991. Actividade Ígnea Mesozóica em Portugal., Tese de Doutoramento, Faculdade de Ciências da Univeridade de Lisboa. Ph.D. thesis.*
- *Miranda, R., Valadares, V., Terrinha, P., Mata, J., Azevedo, M.d.R., Gaspar, M., Kullberg, J.C., Ribeiro, C., 2009. Age constrains on the Late Cretaceous alkaline magmatism on the West Iberian Margin. Cretaceous Res. 30, 575 – 586.*
- *Panozzo, R.H., 1984. Two-dimensional strain from the orientation of lines in a plane. J. Struct. Geol. 6, 215 – 221.*
- *Panozzo, R.H., 1983. Two-dimensional analysis of shape-fabric using projections of digitized lines in a plane. Tectonophysics 95 (3-4), 279 – 294.*
- *Passchier, C., and Trouw, R., 2005. Microtectonics, second ed. Springer, Berlin, New York, pp 366.*
- *Peach, C., Spiers, C., Trimby, P., 2001. Effect of confining pressure on dilatation, recrystallization, and flow of rock salt at 150 °C. Jo J. Geophys. Res. 106, 13315 – 13328.*
- *Pennock, G.M., Drury, M.R., Spiers, C.J., 2005. The development of subgrain misorientations with strain in dry synthetic NaCl measured using EBSD. J. Struct. Geol. 27, 2159 – 2170.*
- *Pennock, G.M., Drury, M.R., Peach, C.J., Spiers, C.J., 2006a. The influence of water on deformation microstructures and textures in synthetic NaCl measured using EBSD. J. Struct. Geol. 28, 588 – 601.*
- *Pennock, G. M., Drury, M. R., Spiers, C. J. 2006b. Grain boundary populations in wet and dry NaCl. Materials Science and Technology 22 (11), 1307 – 1315.*
- *Pollard, D.D., 1987. Elementary fracture mechanics applied to the structural interpretation of dykes. in: Halls, H.C., Fahrig, W.F. (Eds.), Mafic dyke Swarms: Geological Society of Canada, Special Paper, 34, 5 – 24.*
- *Raposo, M.I.B., and Ernesto, M. 1995. Anisotropy of magnetic-susceptibility in the Ponta-Grossa Dyke Swarm (Brazil) and its relationship with magma flow direction, Phys. Earth Planet. Int., 87(3-4), 183 – 196.*
- *Renner, J., Evans, B., Hirth, G. 2000. On the rheologically critical melt fraction, Earth Planet. Sc. Lett. 181(4), 585 – 594.*
- *Ribeiro, P., Silva, P.F., Moita, P. Kratinová, Z., Marques, F.O., Henry, B., 2013. Palaeomagnetism in the Sines massif revisited – Evidences for Late Cretaceous widespread hydrothermal alteration and associated partial remagnetization. Geophys. J. Internat. 195(1), 176 – 191.*
- *Rochette, P., Jenatton, L., Dupuy, C., Boudier, F., Reuber, I. 1991. Diabase dikes emplacement in the oman ophiolite - a magnetic fabric study with reference to geochemistry. in: Peters, T.J., Nicolas, A., Coleman, R.G. (Eds.), Ophiolite Genesis And Evolution of The Oceanic Lithosphere, Petrology and Structural Geology 5, Kluwer Academic Publishers, Dordrecht, 55 – 82.*

- *Rubin, A.M., 1993. Tensile fracture of rock at high confining pressure: implications for dike propagation. J. Geophys. Res. 98, 15919 – 15935.*

- *Rubin, A.M., 1995. Propagation of magma-filled cracks. Annual Review of Earth and Planetary Science 23, 287 – 336.*

- *Schléder, Z., and Urai, J.L., 2005. Microstructural evolution of deformationmodified primary halite from the Middle Triassic Röt Formation at Hengelo, The Netherlands. Int. J. Earth Sci. 94 (5-6), 941 – 955.*

- *Schléder, Z., and Urai, J., 2007. Deformation and recrystallization mechanisms in mylonitic shear zones in naturally deformed extrusive Eocene-Oligocene rocksalt from Eyvanekey plateau and Garmsar hills (central Iran). J. Struct. Geol. 29, 241 – 255.*

- *Schléder, Z., Burliga, S., Urai, J.L., 2007. Dynamic and static recrystallization-related microstructures in halite samples from the Klodawa salt wall (central Poland) as revealed by gamma-irradiation. Neues Jb. Miner. Abh. 184 (1), 17 – 28.*

- *Silva, P. F., Henry, B., Marques, F. O., Font, E., Mateus, A., Vegas, R., Miranda, J. M., Palomino, R., Palencia-Ortas, A. 2008. Magma flow, exsolution processes, and rock metasomatism in the Great Messejana-Plasencia dyke (Iberian Peninsula). Geophys. J. Int. 175, 806 – 824.*

- *Silva, P. F., Marques, F. O., Machek, M., Henry B., Hirt, A.M., Roxerová, Z., Madureira, P., Vratislav, S. 2014. Evidence for non-coaxiality of ferrimagnetic and paramagnetic fabrics, developed during magma flow and cooling in a thick mafic dyke. Tectonophysiscs, this issue.*

- *Storetvedt, K.M., Mitchell, J.C., Abranches, M.C., Oftedahl, S., 1990. A new kinematic model for Iberia; further palaeomagnetic and isotopic age evidence, Phys. Earth Planet. Inter. 62, 109 – 125.*

- *Tarling D.H., and Hrouda F., 1993. The Magnetic Anisotropy of Rocks. Chapman and Hall, London. Terrinha, P., 1998. Structural geology and tectonic evolution of the Algarve Basin. PhD thesis, Imperial College, University of London, U.K., pp 428.*

- *Terrinha, P.A.G., Coward, M.P., Ribeiro, A., 1990. Salt tectonics in the Algarve Basin: the Loulé diapir. Comunicações dos Serviços Geológicos de Portugal t.76, 33 – 40.*

- *Terrinha P., Ribeiro A., Coward M. P., 1994. Mesoscopic structures in a salt wall. The Loulé salt wall diapir, Algarve Basin, south Portugal, Salt Tectonics meeting, Geological Society (14 15th September 1994, London), abstract.*

- *Ter Heege, J.H., De Bresser, J.H.P., Spiers, C.J., 2005a. Dynamic recrystallization of wet synthetic polycrystalline halite: dependence of grain size distribution on flow stress, temperature and strain. Tectonophysics 396, 35 – 57.*

- *Ter Heege, J.H., De Bresser, J.H.P., Spiers, C.J., 2005b. Rheological behaviour of synthetic rocksalt: the interplay between water, dynamic recrystallization and deformation mechanisms. J. Struct. Geol. 27 (6), 948 – 963.*

- *Trimby, P.W., Drury, M.R., Spiers, C.J., 2000. Recognising the crystallographic signature of recrystallization processes in deformed rocks: a study of experimentally deformed rocksalt. J. Struct. Geol. 22 (11–12), 1609 – 1620.*

- *Urai, J., Spiers, C., Peach, C., Franssen, R., Liezenberg, J., 1987. Deformation mechanisms operating in naturally deformed halite rocks as deduced from microstructural investigations. Geologie en Mijnbouw 66, 165 – 176.*

- *Urai, J., Spiers, C., Zwart, H., Lister, G., 1986. Weakening of rocksalt by water during long term creep. Nature 324, 554 – 557.*

- *Urai, J.L., Schléder, Z., Spiers, C.J., Kukla, P.A., 2008. Flow and transport properties of salt rocks, in: Littke, R., Bayer, U., Gajewski, D., Brink, H.J., Winter, I. (Eds.), Dynamics of Complex Intracontinental Basins: The Central European Basin System, 2 – 5.*
- *Van der Voo, R., 1969. Paleomagnetic evidence for the rotation of the Iberian Peninsula. Tectonophysics 7, 5 – 56.*
- *Verwey, E.J., 1939. Electronic conduction of magnetite (Fe3O4) and its transition point at low temperature. Nature 144, 327 – 328.*
- *Wang, D., and Van der Voo R., 2004. The hysteresis properties of multidomain magnetite and titanomagnetite/titanomaghemite in mid-ocean ridge basalts. Earth Planet. Sci. Lett. 220, 175 – 184.*
- *Weinberger, R., Baer, G., Shamir, G. and Agnon, A., 1995. Deformation bands associated with dyke propagation in porous sandstone, Makhtesh Ramon, Israel, in Physics and Chemistry of Dykes, edited by G. Baer and A. Heimann, A.A. Balkema, Brookfield, Vt. pp. 95 – 112.*
- *Wenk, H.-R., Armann, M., Burlini, L., Kunze, K., Bortolotti, M., 2009. Large strain shearingof halite: experimental and theoretical evidence for dynamic texture changes. Earth Planet. Sci. Lett. 280, 205 – 210.*
- *Wilson, R.I., Haggerty, S.E., Watkins, N.D., 1968. Variation of paleomagnetic stability and other parameters in a vertical traverse of a single Icelandic lava. Geophys. J.R. astr. Soc. 16, 79 – 96.*
- *Závada, P., K. Schulmann, J. Konopásek, S. Ulrich, Lexa, O., 2007. Extreme ductility of feldspar aggregates—Melt enhanced grain boundary sliding and creep failure: Rheological implications for felsic lower crust. J. Geophys. Res. 112, B10210,*
- *Závada, P., Desbois, G., Schwedt, A., Lexa, O. & Urai, J. L. 2012. Extreme ductile deformation of fine-grained salt by coupled solution-precipitation creep and microcracking: Microstructural evidence from perennial Zechstein sequence (Neuhof salt mine, Germany), J. Struct. Geol. 37, 89 – 104.*